HAL
open science

Multiphysical Characteristics of Limestones for Energy-Efficient and Sustainable Buildings Components

Tristan Pestre, Emmanuel Antczak, Franck Brachelet, Didier Pallix

To cite this version:

Tristan Pestre, Emmanuel Antczak, Franck Brachelet, Didier Pallix. Multiphysical Characteristics of Limestones for Energy-Efficient and Sustainable Buildings Components. Journal of Materials in Civil Engineering, 2022, 34 (4), 10.1061/(ASCE)MT.1943-5533.0004158 . hal-03627225v3

HAL Id: hal-03627225

https://univ-artois.hal.science/hal-03627225v3

Submitted on 3 Jul 2023

HAL is a multi-disciplinary open access archive for the deposit and dissemination of scientific research documents, whether they are published or not. The documents may come from teaching and research institutions in France or abroad, or from public or private research centers.

L'archive ouverte pluridisciplinaire **HAL**, est destinée au dépôt et à la diffusion de documents scientifiques de niveau recherche, publiés ou non, émanant des établissements d'enseignement et de recherche français ou étrangers, des laboratoires publics ou privés.

Copyright

Multi-physical characteristics of limestones for energy-efficient and sustainable buildings components

Tristan PESTRE[1] ; Emmanuel ANTCZAK[2] ; Franck BRACHELET[3] ; Didier PALLIX[4]

[1]Research Engineer, Univ. Artois, Univ. Lille, Institut Mines-Télécom, Junia, ULR 4515–LGCgE, Laboratoire de Génie Civil et géo-Environnement, F-62400 Béthune, France (corresponding author). ORCID: https://orcid.org/0000-0003-0104-2280. Email: tristan.pestre@gmail.com.

[2]Professor, Univ. Artois, Univ. Lille, Institut Mines-Télécom, Junia, ULR 4515–LGCgE, Laboratoire de Génie Civil et géo-Environnement, F-62400 Béthune, France. Email: emmanuel.antczak@univ-artois.fr.

[3]Research Engineer, Univ. Artois, Univ. Lille, Institut Mines-Télécom, Junia, ULR 4515–LGCgE, Laboratoire de Génie Civil et géo-Environnement, F-62400 Béthune, France. Email: franck.brachelet@univ-artois.fr.

[4]Deputy Managing Director, Technical Center for Natural Building Materials, 17 Letellier St., 75015 Paris, France. Email: pallix.d@ctmnc.fr.

Note. This manuscript was submitted on May 19, 2021; approved on August 23, 2021; published online on January 21, 2022, in the Journal of Materials in Civil Engineering, (ASCE, ISSN 0899-1561). In this third HAL release, a correction has been applied to "Rc" values in Table 13 that contained errors.

ABSTRACT

Natural stone is a traditional building material, used worldwide for millennia. Its mechanical properties are rather well known, but only a small quantity of data is available regarding its hygrothermal characteristics. However, these characteristics are essential for the design of energy efficient buildings. Stones are in fact associated with insulation materials, which strongly modify the hygrothermal behavior of building walls, thereby impacting their durability and thermal comfort. This study focuses on the hygrothermal characterization of a dozen samples of limestone, offering an adequate representation of their use across France. Thermal conductivity and heat capacity, sorption and desorption isotherms, water vapor permeability, and moisture buffer value (MBV) were all notably determined and analyzed. These data can then be used to model heat and mass transfers in building walls. Limestone features extensive physical properties that can vary from one place to another within the same quarry. A statistical classification, according to mechanical properties of thousands of French limestones has also been carried out. This classification allows estimating the hygrothermal properties previously determined for other stones.

INTRODUCTION

The mechanical properties of natural stones, as well as their durability, aesthetic qualities and local production possibilities have made them traditional building materials renowned in many parts of the world. France possesses some 570 stone quarries for the production of ornamental and/or construction rocks, most of which are limestone and granite. Limestone is ideally suited to the construction of infrastructure and buildings, while granite is more commonly used in the road works sector and for funerary objects (Dessandier et al. 2014). A large proportion of built facilities still existing in France incorporates stone elements in the form of masonry, roofing, interior or exterior coverings. Limestone has been preferred for its medium hardness and ease of cutting. These structures, whether exceptional or modest, have survived centuries of history. Limestone has been used since Gallo-Roman times for the construction of religious and public buildings (cathedrals, amphitheaters, bridges, etc.), both during the Renaissance period (Loire Valley castles) and under the Second Empire when Baron Haussmann built his wide “Grands Boulevards” and buildings that still shape the Paris cityscape, undoubtedly the world's most characteristic limestone architecture.

Today, in order to face the challenges of climate change and meet the international objectives set in terms of sustainable development during the 2015 Paris Agreement (UNFCCC 2021), energy policies aimed at reducing consumption and greenhouse gas emissions have been implemented across all economic and industrial sectors. In France, thermal regulations adopted for construction will further advance the move towards low-energy buildings and a moderate environmental impact on their full life cycle (French Republic 2018). New buildings will need to produce as much or even more energy than they consume, and their environmental impacts will be assessed by means of analyses (LCA) that include in particular the contribution of construction products and equipment. Older buildings, by far more numerous than newer ones, will have to be renovated to achieve the thermal regulation targets assigned for existing buildings.

In this context, future French environmental regulation RE 2020 (French Republic 2021) will seek to encourage the use of natural, bio-based, or agro-based construction materials, which generally require minor initial transformation and moreover allow for ease of recycling. Natural limestone, once commonly used in building construction but had been overtaken by masonry such as concrete or clay block, is now tending to reappear as a construction product adapted to regulatory requirements.

With improvements in the thermal and airtightness performance of buildings, it has become essential to know the hygrothermal characteristics of the materials composing building walls (Mendell et al. 2018), including structural and insulation materials. This advancement should make it possible to ensure buildings' sustainability and energy performance, in addition to improving the thermal comfort and health of occupants (Ortiz et al. 2020) while minimizing the environmental impact of structures. Many studies have shown that water in liquid or vapor form is a vector responsible for an extensive amount of damage (Beck 2006). Insufficient moisture discharge can also lead to health risks linked to the development of allergenic microorganisms (Abadie et al. 2013). Apart from accidental infiltration, moisture accumulation can be caused by thermal bridges, condensation zones, an inadequate air exchange rate or the use of materials with unsuitable hygrothermal properties. Specific materials, especially bio-sourced or natural, are known to regulate ambient humidity more effectively (Rode et al. 2005). Regarding limestone, its physical and mechanical properties are relatively well known (Kourkoulis et al. 2006), even though its origins are multiple due to the many extraction sites. In contrast, the hygrothermal characteristics are far more difficult to obtain; given the time-consuming nature of experimental protocols, it is impossible to characterize the entirety of limestone available throughout France. In literature, few studies have dealt simultaneously with the thermal and moisture properties of natural stone.

Our investigation was based on the material, independent of the construction system. Indeed, to simulate heat and moisture transfer in a wall made of multiple materials, it is preferable to know precisely the respective properties of all its components. Other methods allow determining, in a nondestructive and in situ, the thermal properties of existing building walls (Lucchi 2017; Pascucci and Lucchi 2016; Litti et al. 2015). Comparison of numerical simulation results with experimental results shows that reliable data on the properties of the materials are necessary to minimize prediction errors.

To better understand the behavior of this building material, a descriptive statistical study of the mechanical properties of rocks was carried out using the Technical Center for Natural Building Materials (CTMNC) database. Such an effort developed a better knowledge of the wide array of rocks' main mechanical characteristics (uniaxial compressive strength and deflection under a centered load) with respect to elementary variables, such as apparent density and open porosity. This study was supplemented by a statistical classification, thus enabling the creation of families of rocks with similar physical properties. Consequently, these families or classes offer more suitable alternatives than traditional petrographic classifications (e.g. those of Folk 1959 and Dunham 1962) when treating problems related to the building sector. From this classification, a dozen French limestones were selected according to various parameters, i.e. historical and contemporary use in construction, geographic origin, geological age, range of densities, and distribution within the identified classes.

Based on this selection of limestones, a major measurement campaign could be conducted, including thermal properties (thermal conductivity, heat capacity, thermal diffusivity, thermal effusivity) and hygrothermal characteristics (sorption/desorption isotherms, the Moisture Buffer Value, water vapor permeability, and water absorption at atmospheric pressure). The experimental protocols are difficult to execute due to the slowness of both heat and moisture transfers. It proved to be important however to record the hygrothermal properties of limestones over the entire range of potential relative humidity values, from RH=0% to RH=100%. This classification will make it possible to estimate the hygrothermal properties of other limestones belonging to the same family as those tested. The data obtained on thermal and hydric characteristics then should be used as input to the numerical models developed for coupled heat and moisture transfers in studies on building walls.

STATISTICAL ANALYSIS OF LIMESTONE

The extent of physical-mechanical properties

The CTMNC has developed a database on stones, called the Lithoscope© (CTMNC 2021), integrating nearly 120 limestone and marble limestone rocks from French quarries. Some of these entries have been characterized more than once, over a number of years. A total of 450 data pairs are available, comprising four variables, namely: bulk density "ρ" [kg/m^3], open porosity "n" [%], bending strength under centered load "Rf" [MPa], and uniaxial compressive strength "Rc" [MPa]. A simple observation of these variables already indicates the extent of the mechanical characteristics of natural limestones. **Fig. 1** shows the obtained box plots, which represent the range of each variable with their minimum and maximum values, as well as the mean (cross) and three quartiles (horizontal lines).

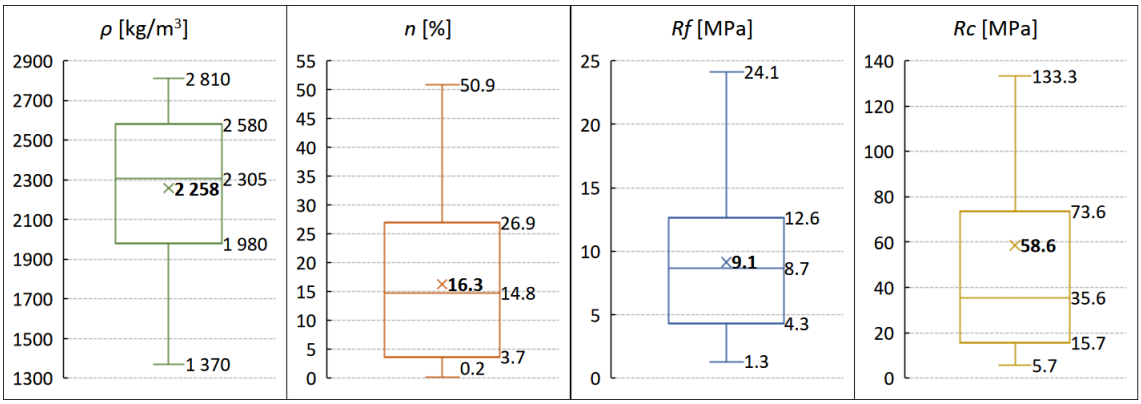

Fig. 1 The extent of mechanical properties of limestone

With compressive strengths ranging from 6 MPa to 130 MPa and open porosities of nearly 0% to 50%, the limestone geological family can support many types of construction and ornamental uses, whether interior or exterior, decorative or structural. In examining the distributions, it can be noticed that roughly 50% of the stones have values above or below the average for "ρ", "n", and "Rf" (the average is approximately equal to the median). Yet for "Rc", 50% of the stones have a value less than 35.6 MPa, which is lower than the average, thus indicating that a limited quantity of stones has distinctly higher compressive strengths. The densest and least porous limestones are generally called "marble" and tend to be used more like actual marble (flooring, furniture, decoration). For all stones, the bending strength corresponds on average to 18.5% of the compressive strength (Rf/Rc ratio), or: $R_c \approx 5.4 \times R_f$ (1). By associating these variables, correlations can be drawn (**Fig. 2**) and, after modeling, relationships can be established to estimate the physical properties of limestone that is uncharacterized yet for which at least one characteristic is known.

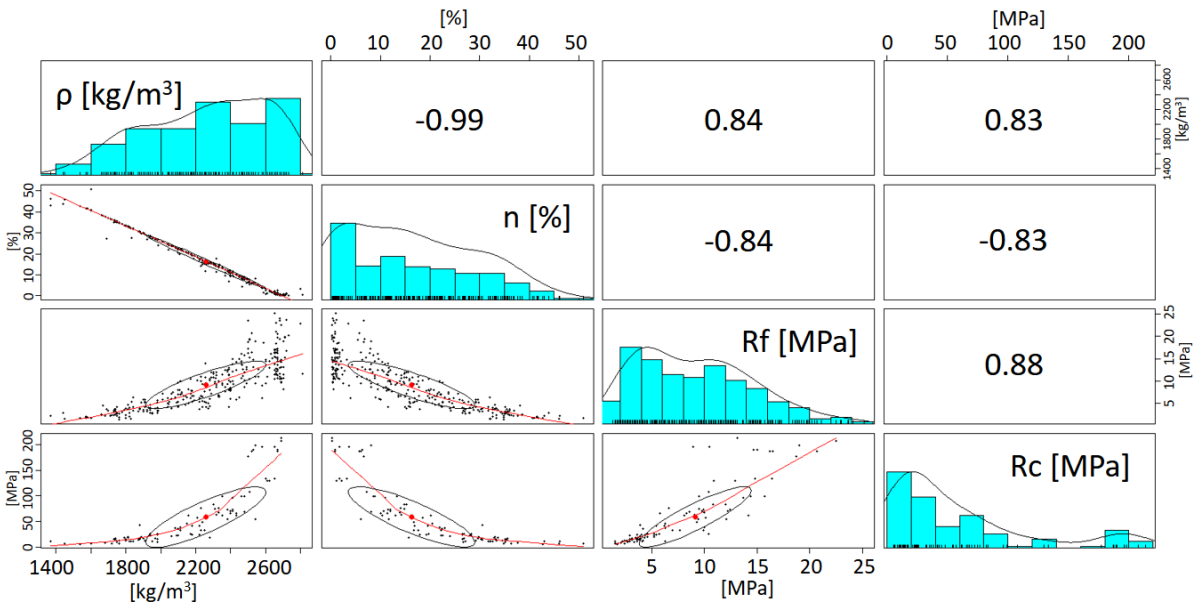

Fig. 2 Correlations between limestone properties

The closer the correlation coefficient is to 1 or -1, the more positively or negatively correlated the indicators, respectively. Conversely, a value near 0 implies a lack of correlation between the indicators. Bulk density is the simplest physical property to obtain experimentally. According to this figure, it is strongly correlated with open porosity, and their relationship seems to be linear. Open porosity actually represents the amount of voids in the solid matrix of the material, while conversely density depends on the mass and thus on the amount of material per unit volume. A negative correlation coefficient means that an increase in one variable is linked to a decrease in the other. This observation is similar for the other variables, with negative correlation coefficients between porosity and mechanical strength and positive coefficients when compared with density. An increase in density is therefore generally tied to an increase in mechanical strength and *vice versa* for open porosity. These trends between density or porosity and flexural or compressive strength appear to be exponential. Between the two strengths, it is difficult to conclude on a linear relationship given the significant dispersion, especially for the higher value. However, the relatively high positive correlation coefficient means that the increase in flexural strength is often associated with an increase in compressive strength.

Regression modeling results are presented in **TABLE 1**. To describe the quality of this model, we have relied on the coefficient of determination, which expresses the percentage of variation explained by the model, as well as on the RMSE value to assess the dispersion of prediction quality.

TABLE 1. Estimation of the physical properties of limestones

Equation	a	b	R^2 (linear)	RMSE
$n = a.\rho + b$	-0.0368	99.36	0.989	1.340
$\rho = a.n + b$	-26.87	2695	0.989	36.20
$Rc = a.Rf + b$	10.469	-20.75	0.778	27.72
$Rf = a.Rc + b$	0.0743	3.225	0.778	2.335
$Rf = a.b^{\rho}$	0.1303	1.0018	0.814	2.894
$Rf = a.b^{n}$	16.381	0.9526	0.819	2.869
$Rc = a.b^{\rho}$	0.0698	1.0029	0.869	24.58
$Rc = a.b^{n}$	183.95	0.9242	0.873	23.94

Let us note that the coefficient of determination is high between bulk density and open porosity, which can therefore be estimated with satisfactory accuracy. More care is needed however in estimating the other variables, especially between the flexural and compressive strengths.

Statistical classification

A classification according to physical properties can be useful in the field of construction, where the geological nature of a stone is less critical than, for example, its mechanical strength or density. To carry out this classification, we chose the k-means unsupervised classification method. A bibliographical study showed that this classification method has been used on rocks in a petroleum context (Popielski et al. 2012), and for building engineering (Akil et al. 2019). This method seeks to group statistical individuals, without any *a priori* information, according to a chosen metric, e.g. the Euclidean distance around "*k*" representative individuals, which are the centroids of the clusters formed; the number "*k*" of classes must be fixed. It has been decided herein that this choice should be automatic. In this regard, the Davies-Bouldin and Silhouette methods yielded the optimal number of five classes for the 130 data pairs with four known variables (ρ, n, Rf, Rc). This ranking is explained by a decision tree, as diagrammed in **TABLE 2**.

TABLE 2 Decision tree of the obtained statistical classes

Class n°	ρ [kg/m^3]	n [%]	Type of limestone
Class 1	$\rho > 2480$	-	Cold
Class 2	$2250 < \rho \leq 2480$	-	Hard
Class 3	$1980 < \rho \leq 2250$	-	Firm
Class 4	$\rho \leq 1980$	$n \leq 36.3$	Half-firm
Class 5	$\rho \leq 1980$	$n > 36.3$	Soft

From a practical point of view, it is worth noting that the classification according to stone identification number (Martinet and Quénée 2008) has also been divided into five families: soft stones, half-firm, firm, hard, and cold. In the standard on hygrothermal properties, under the tabulated useful values (ISO 2007), limestone is separated into six classes differentiated by density. The last column of **TABLE 2** lists the interpreted equivalence of our results with respect to these two classifications. The main difference is found between Classes 4 and 5, which in our case are distinguished by their open porosities and not by their densities. A physical explanation could be that below a certain density, porosity provides a better indication of the mechanical properties than density, or else that the number of samples in these classes (in particular, Class 5) is too limited. Moreover, it is possible to use these results to determine the physical class of each new stone, as needed to integrate the characteristics of the new stone into the decision tree (predictive model), to obtain its class.

Sample selection

In this research work, twelve limestone rocks from Metropolitan France (**Fig. 3**) were selected for the characterization campaign: Beaulieu (BEA), Borrèze (BOR), Brétignac (BRE), Euville (EUV), Nogent-sur-Oise (NOG), Noyant (NOY), Paussac (PAU), Savonnières (SAV), Saint-Vaast Fine (SVF), Tervoux (TER), Tuffeau (TUF), and Vers-Pont-du-Gard (VPG) stone.

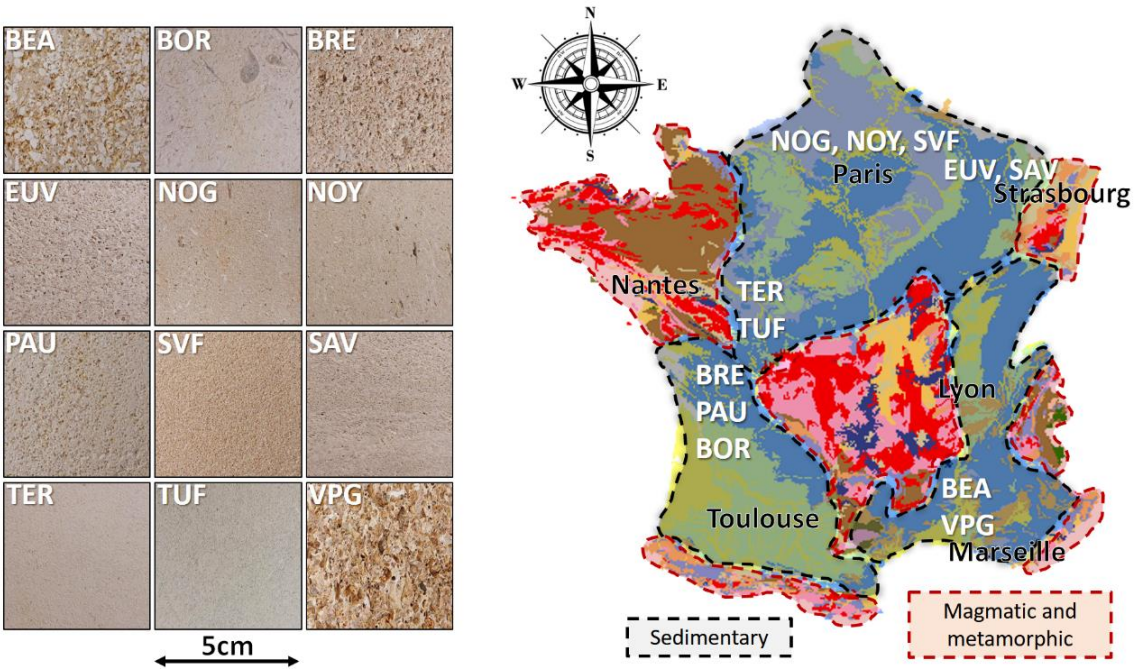

Fig. 3 Simplified geological map of France with selected samples

Aged from 14 Ma to 166 Ma, they are on the whole representative of stones found in masonry. These stones have been placed in many existing structures over the centuries (castles, religious buildings, homes, etc.) and continue to be used today (apartment buildings, tertiary buildings, single-family dwellings).

Most tests were performed in accordance with standardized norms and protocols to accommodate and compare the data. The dry bulk density "ρ_0" [kg/m^3] and open porosity "n" [%] of these stones were determined according to the EN 1936 standard (CEN 2006). These preliminary physical characteristics allow classifying the samples as per the previously determined predictive model.

TABLE 3 reveals that the stones are distributed among classes 3, 4 and 5, which makes for good representativeness. The limestones of classes 1 and 2 are harder and their use is favored for coatings, paving, furnishing and decoration. These are called marble stones due to their ease of polishing even though they do not belong to this geological class; they are less used in masonry than the other classes (3, 4 and 5).

TABLE 3 Classification of the studied stones

Limestone	ρ_0 [kg/m^3]	n [%]	Statistical class
BEA	1842	31.6	4
BOR	2181	14.1	3
BRE	1927	28.5	4
EUV	2215	17	3
NOG	1649	37.7	5
NOY	1761	34.5	4
PAU	1898	28.1	4
SVF	1520	43.4	5
SAV	1855	31.4	4
TER	2043	23.7	3
TUF	1390	44.4	5
VPG	1833	32.6	4

HYDRIC CHARACTERIZATION

Basic characteristics, i.e. density, porosity, water absorption at atmospheric pressure and capillarity, were first determined for the twelve selected stones. Water absorption at atmospheric pressure, determined according to the EN 13755 standard (CEN 2008), allows identifying the maximum water content contained by the stone under the effect of ambient pressure. This value is representative of what a real building wall can undergo under the most unfavorable humidity conditions. The maximum water content then serves to calculate the degree of saturation of a wet stone. Outside of the standard, the accessible porosity at atmospheric pressure "n_{acc}" [%] can be derived from this test. The water content of a material "w" [kg/m^3] is found by measuring the mass of water contained therein "Δm" [kg], with its dry mass "m_{dry}" [kg], multiplied by the dry density of the material "ρ_0" [kg/m^3].

$$w_{sat} = \frac{m_{sat} - m_{dry}}{m_{dry}} \times \rho_0 \tag{2}$$

It is therefore necessary to determine the dry mass of the samples in order to deduce the dry bulk density. Specimens must be dried at 70°C to constant mass (about 48 h). Next, cooled specimens are immersed in water until saturation; they are then weighed at regular intervals to track the evolution of mass and ensure stability at the end of the test. Accessible porosity is the ratio between water content and density of the water; it does not correspond exactly to the open porosity since the latter is derived under vacuum. Pressure conditions differ, as do the results, yet a correlation does appear to exist.

$$n_{acc} = \frac{w_{sat}}{\rho_w} \tag{3}$$

The coefficient of water absorption "A" [kg/(m².s$^{0.5}$)] corresponds to the mass of water absorbed "Δm" [kg] per unit area "S" [m²] with respect to the square root of time "t" [s]. It is calculated according to Standards EN 772-11 and EN 771-6 (CEN 2011; 2015). The underside of the test piece is immersed in water, which rises by means of capillary action, thus increasing its mass over time. This parameter is rather useful since it specifically allows estimating the coefficient of diffusion of liquid water for the study of mass transfer (Künzel 1995); for the case herein, it is given perpendicular "⊥" and parallel "//" to the sedimentation layers. Results are presented in **TABLE 4** for each of the twelve stones studied.

$$A = \frac{m_{wet} - m_{dry}}{S.\sqrt{t}} \tag{4}$$

TABLE 4 Water absorption at atmospheric pressure and porosity

Limestone	ρ_0 [kg/m^3]	w_{sat} [kg/m^3]	n_{acc} [%]	A// [g/(m².s0,5)]	A⊥ [g/(m².s0,5)]
BEA	1842	247	24.7	488	430
BOR	2181	162	16.2	119	119
BRE	1927	215	21.5	285	260
EUV	2215	93.6	9.36	71	42
NOG	1649	268	26.8	296	273
NOY	1761	248	24.9	99	96
PAU	1898	217	21.7	328	293
SVF	1520	310	31.0	1090	980
SAV	1855	111	11.1	67	36
TER	2043	214	21.4	169	164
TUF	1390	334	33.4	426	399
VPG	1833	203	20.4	99	68

Densities range from 1390 [kg/m^3] to 2215 [kg/m^3] with an average of 1843 [kg/m^3]. The range of open porosity values is also extensive, with a minimum of 14.1% and a maximum of 44.4%, for an average of 30.6%. Water absorption at atmospheric pressure is strongly correlated with both open porosity and dry bulk density, which is logical; the corresponding correlation coefficients are respectively 0.86 and -0.92. Stones with a greater water holding capacity (high w_{sat}) are those with the highest water absorption coefficients "A". However, the pore network does exert an influence since the TUF stone has, for example, a greater water content at saturation than the SVF stone, while the latter is more capillary. The two stones of the sample with the most extreme properties are TUF and EUV, categorized respectively in classes 5 and 3. The BEA and VPG stones lie close to the average sample values and are positioned in class 4.

Moisture Buffer Value

The moisture buffer value (MBV) was determined according to the NORDTEST Protocol issued by the Technical University of Denmark (Rode et al. 2005). This test provides information on the dynamic hydric behavior of materials. The *MBV*, expressed in [g/(m².%$_{RH}$)], corresponds to the quantity of water that the material will store or destock per unit of surface area and relative humidity; it thus represents the capacity of hydrous material regulation, or "hydrous inertia".

This measure is the result of a dynamic test, whose principle consists of exposing two faces of a rectangular parallelepiped specimen to 24-hour cycles during which the relative humidity alternates between dry and wet. We used a BINDER MKF115 (Tuttlingen, Germany) environmental chamber (-40°C to +180°C and 10%RH to 98%RH, with accuracy of ±2.5%RH and ±0.1°C to ±0.6°C). This same chamber was also used to determine the sorption isotherms and water vapor transmission properties. The specimen's other sides are waterproofed with aluminized adhesive tape. Instructions call for 33% relative humidity for 16 hours and 75% for 8 hours. These exposures correspond to the conditions likely found in inhabited rooms during part of the day or night, e.g. bedrooms or offices.

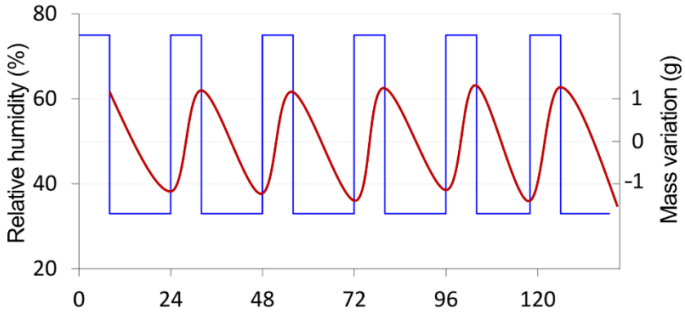

Fig. 4 Example of experimental results (TUF stone)

Two values are derived, in adsorption "ads" and desorption "des", depending on: the difference in mass "Δ*m*" [g], exposed surface area "*S*" [m²], and the difference in relative humidity "Δ*RH*" [-]. An example of an experimental survey is shown in (**Fig. 4**); the average value characterizes the effective MBV of the material.

$$MBV_{mean} = \left(\frac{\Delta m_{ads}}{S.\Delta RH} + \frac{\Delta m_{des}}{S.\Delta RH}\right) \times \frac{1}{2} \quad (5)$$

The test was conducted at two different temperatures: 13°C and 23°C. The standard protocol recommends 23°C, but the 13°C value demonstrates the influence of temperature on the results (**TABLE 5**).

TABLE 5 MBV value for 23°C and 13°C

MBV [g/(m².%RH)]	MBV_{ads} @23°C	MBV_{des} @23°C	MBV_{mean} @23°C	MBV_{ads} @13°C	MBV_{des} @13°C	MBV_{mean} @13°C
BEA	0.42	0.44	**0.43**	0.33	0.31	**0.32**
BOR	0.27	0.29	**0.28**	0.22	0.19	**0.21**
BRE	0.44	0.45	**0.45**	0.32	0.29	**0.31**
EUV	0.18	0.20	**0.19**	0.15	0.13	**0.14**
NOG	0.56	0.57	**0.56**	0.45	0.45	**0.45**
NOY	1.09	1.10	**1.10**	0.84	0.81	**0.83**
PAU	0.29	0.29	**0.29**	0.23	0.21	**0.22**
SVF	0.63	0.65	**0.64**	0.49	0.47	**0.48**
SAV	0.19	0.21	**0.20**	0.15	0.12	**0.13**
TER	0.33	0.34	**0.34**	0.25	0.22	**0.24**
TUF	2.67	2.66	**2.66**	2.12	2.11	**2.12**
VPG	0.69	0.71	**0.70**	0.49	0.48	**0.49**

The protocol proposes classifying the results into five categories, ranging from negligible to excellent (**TABLE 6**), which yields a simple interpretation of results, as well as a comparison with other materials.

TABLE 6 Ranges for practical Moisture Buffer Value classes.

MBV practical class @23°C (8h/16h)	Minimum MBV level	Maximum MBV level	Results for limestones
Negligible	0	0.2	EUV
Limited	0.2	0.5	BEA, BOR, BRE, PAU, SAV, TER
Moderate	0.5	1.0	NOG, SVF, VPG
Good	1.0	2.0	NOY
Excellent	2.0	> 2.0	TUF

Let us note that our twelve samples are present in each class. The minimum value of 0.19 [g/(m².%$_{RH}$)] is reached for the EUV stone and the maximum value of 2.66 [g/(m².%$_{RH}$)] for the TUF stone; the majority of stones belong to the "limited" and "moderate" categories. Placed inside a built structure, some stones can contribute to effectively regulating the ambient relative humidity and improving the comfort of occupants. As a means of comparison, hemp concrete would possess an MBV of 2.18 [g/(m².%$_{RH}$)] according to (Asli 2017). Laterite, a clay rock derived from the decomposition of other rocks, would possess an MBV between 2.65 and 2.95 [g/(m².%$_{RH}$)] according to (Abhilash et al. 2016). According to (Rode et al. 2005), the MBV of concrete is roughly equal to 0.40 [g/(m².%$_{RH}$)] and that of gypsum board to 0.60 [g/(m².%$_{RH}$)]. Once the temperature decreases, the amount of water vapor potentially contained in air also decreases; it is thus logical to note that the MBV at 13°C is lower than that at 23°C.

Water vapor permeability

The water vapor transmission properties were determined according to ISO 12572 (ISO 2016). The experimental protocol is based on the use of water vapor-tight cups to accommodate test specimens, while remaining hermetically sealed on their periphery. Inside the cups, desiccant solution "dry cups" or saturating "wet cups" are installed. The set composed of the cup, the solution and the specimen is then placed in a climate-controlled chamber regulated at a temperature of 23°C and a relative humidity of 50%. The mass flow rate of steam "g" [kg/(m².s)] is calculated from the evolution of mass, which is evaluated by means of regular weighing. The dynamics of the mass difference must be monitored during the test in order to verify the good performance of the desiccant or saturant solutions. The vapor surface flow rate is calculated from the variation in mass "m" [kg] during time interval "t" [s] between weighings, as well as from the surface area of vapor passing in specimen "S" [m²] of the specimen exposed to water vapor.

$$g = \frac{m_2 - m_1}{S \times (t_2 - t_1)} \tag{6}$$

The water vapor permeability "δ" [kg/(m.s.Pa)] is calculated from: the vapor mass flow rate "g", the vapor pressure difference "p" [Pa] on both sides of the test piece, and the test piece thickness "e" [m]. The vapor pressure difference is dependent on the relative humidity difference; relative humidity is indeed the ratio between vapor pressure and saturation vapor pressure.

$$\delta = \frac{g.e}{\Delta p} \tag{7}$$

The water vapor resistance factor "μ" [-] is often preferred in the field of building engineering; its orders of magnitude are better known than those of permeability. This factor is determined from the water vapor permeability of the material relative to that of air and can therefore be estimated from the following relationship, where "p_0" and "T" denote respectively the ambient temperature and pressure conditions in [Pa] and [K]. The lower this factor, the more permeable the material to water vapor.

$$\mu = \frac{2.10^{-7} \times T^{0,81}}{\delta . p_0} \tag{8}$$

In our case, the dry and wet cups were performed with respective relative humidity gradients of 0%-50% "dry" and 50%-93% "wet" at 23°C, i.e. with pressure differences of 1,404 Pa and 1,207 Pa (ISO 2016). Thanks to these two tests, the influence of water content on the water vapor permeability of materials can be analyzed. It is important to point out that the values obtained with the wet cup are to be considered with caution as they may integrate a portion of the transfer in liquid form (Künzel 1995).

TABLE 7 Water vapor transmission properties

Limestone	μ "dry" [-]	μ "wet" [-]	δ "dry" [kg/(m.s.Pa)]	δ "wet" [kg/(m.s.Pa)]
BEA	18	11	1.11×10^{-11}	1.67×10^{-11}
BOR	49	31	4.07×10^{-12}	6.33×10^{-12}
BRE	21	17	9.59×10^{-12}	1.18×10^{-11}
EUV	149	56	1.33×10^{-12}	3.51×10^{-12}
NOG	12	9	1.68×10^{-11}	2.13×10^{-11}
NOY	15	9	1.29×10^{-11}	2.12×10^{-11}
PAU	14	13	1.42×10^{-11}	1.49×10^{-11}
SVF	9	7	2.25×10^{-11}	2.82×10^{-11}
SAV	87	48	2.28×10^{-12}	4.13×10^{-12}
TER	22	21	9.06×10^{-12}	9.31×10^{-12}
TUF	9	5	2.09×10^{-11}	3.87×10^{-11}
VPG	32	18	6.22×10^{-12}	1.10×10^{-11}

For the studied stones, the increase in water content systematically causes an increase in water vapor permeability. The ratio between the water vapor permeabilities obtained by the dry and wet cups seems to be similar for a majority of stones, with a coefficient of determination $R^2 = 0.86$. The following equation allows estimating the permeability at a high relative humidity from one at a low relative humidity; it has been derived from a linear regression of the results (**TABLE 7**): $\delta_{wet} = 1.4 \times \delta_{dry} + 2.71 \times 10^{-13}$ (9).

The average vapor diffusion resistance factor of the studied stones equals 36 [-] at low relative humidity and 21 [-] at a higher relative humidity. On average, for all the stones studied, except for the SAV, the values we obtain are 139% lower than the tabulated values of the ISO 10456 (ISO 2007). De Kock et al. (2017) found values between 12.6 and 26.8 (wet cup) for limestones with relatively high density, which seems to confirm our results. However, density is probably not the most representative physical parameter of the water vapor transmission properties, as is shown subsequently (Fig. 14). At low relative humidity, fibrous insulation materials generally display vapor resistance factors between 1 and 10 [-] (Asli 2017), while for concretes the value would lie between 120 and 150 [-] (Abelé et al. 2009). For cementitious materials, these values would be between 45 and 89 [-], according to (Issaadi et al. 2015). The limestones studied thus have overall low water vapor permeabilities for solid structural materials. This characteristic allows the walls to keep perspiring and helps remove excess interior moisture.

Sorption and desorption isotherms

Hygroscopic sorption and desorption isotherms were determined according to ISO 12571 (ISO 2013); they relate the water content of materials to the relative humidity of the air at a given temperature, which has been set at 23°C as per the standard. Specimens, previously dried, weighed, and conditioned, were installed in a climate-controlled chamber regulated for temperature and relative humidity. Increasing levels of relative humidity (sorption) and then decreasing (desorption) were introduced to determine several points on the experimental isotherm. Water content was calculated from each mass measurement. We chose the following steps: 0%, 35%, 50%, 65%, 80%, 90%, and 98%. These steps produced a sufficient number of points, including a majority at high relative humidity, in the area where changes were typically greater (Beck 2006). The level change could only take place once the mass measurements had stabilized. Constant mass was reached when the variation in mass between three consecutive weighings, carried out at least 24 hours apart, was less than 0.1% of the total mass. At least three specimens per type of stone needed to be tested. **Fig. 5** highlights the test durations (10 months for the Noyant stone) along with the various stages completed.

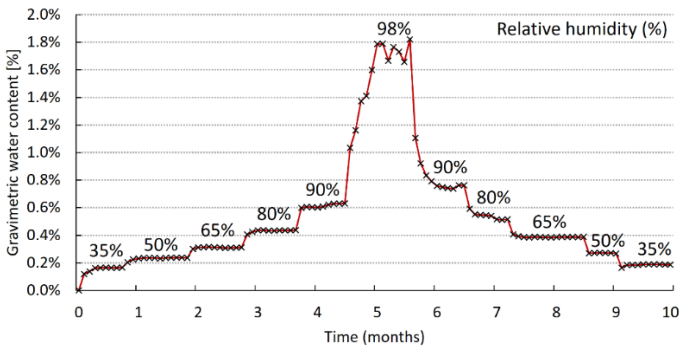

Fig. 5 Example of experimental stages (NOY stone)

The International Union of Pure And Applied Chemistry (IUPAC) provides information to better analyze the various types of sorption isotherms (Sing 1985). Type III sorption isotherms are known to be rare, yet all stones studied appear to fit this category. Isotherms are convex to the x-axis (whether relative humidity or relative pressure) over their entire range and do not show an inflection characteristic of monolayer saturation. Similar results have been obtained by other authors on similar stones or other geological stone configurations, i.e. laterite (Abhilash et al. 2016), limestone (Beck 2006) and sandstone (Rousset Tournier et al. 2001; Zhao and Plagge 2015). The isotherms obtained herein reveal a slight hysteresis, which could be similar to the H3-type hysteresis (Lykiema et al. 1985) characteristic of materials consisting of plate-like aggregates, thus giving rise to slit-like pores. Limestones are in fact formed by sedimentation of successive layers. The degree of saturation is calculated from the effective water content at saturation; it equals between 0 and 1 [-] and serves, among other things, to harmonize the scales and display all twelve isotherms on the same graph (**Fig. 6**).

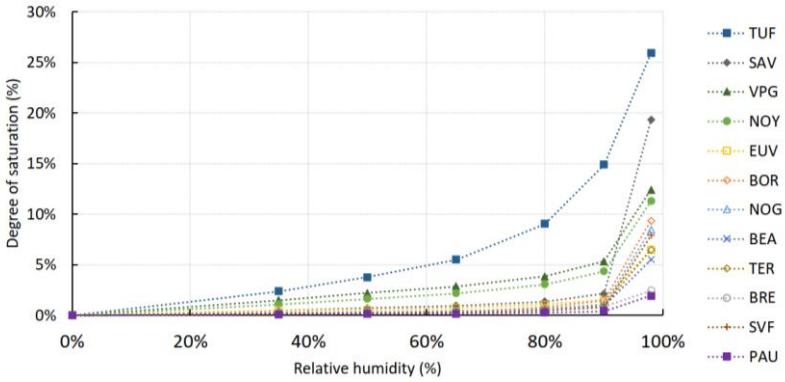

Fig. 6 Sorption isotherms of the twelve samples

TUF stone is the least dense and most porous of the sample; its sorption isotherm clearly demonstrates both its interaction with the relative humidity of air and its large water holding capacity. This finding confirms the results obtained for MBV (**TABLE 5**). EUV stone is the densest and least porous but does not rank last. The pore network has a strong influence on the results. For example, the SVF stone has a high open porosity and relatively low density (**TABLE 3**); however, its pores are granular and fine, making it highly insensitive to the relative humidity in air. Moreover, its saturation water content is high, thus explaining the low degree of saturation. The other counterexample is SAV stone, which has a relatively high open porosity but a low saturation water content; it appears here in second place due to its higher degree of saturation.

Sorption and desorption isotherms modeling

It is possible and very practical to model sorption and desorption isotherms, yielding the relationship between relative humidity and water content of the material, in addition to simulating the water or coupled heat / moisture transfers. The most renowned model, valid over a wide relative humidity range, is GAB (Guggenheim-Anderson-de Boer); it is used in both food (Blahovec and Yanniotis 2010) and civil engineering problems (Colinart et al. 2017). We modeled the sorption and desorption isotherms of all stones using two iterative optimization tools embedded into the Matlab® software. These tools made it possible to fit the experimental and numerical curves by means of the least squares method. The main difference between these two algorithms (i.e. trust-region-reflective "TRR" and Levenberg-Marquardt "LMA") is the possibility or not to set the bounds of the three variables composing the GAB model, namely "X_{12}", "C" and "K", with "w" being the water content [kg/kg] and "RH" the relative humidity [-]. Results obtained are presented in **TABLE 8**.

$$w = \frac{X_{12}.C.K.RH}{(1-K.RH)\times(1-K.RH+C.K.RH)} \tag{10}$$

Variable "X_{12}" [kg/kg] corresponds to the transitional water content between the saturation of the monolayer and the appearance of multilayers. According to (Jannot et al. 2006), this variable would be easier to estimate with the BET model. Variables "C" and "K" [J/mol] are expressed as a function of: the heat of condensation of water "H_l", total sorption of the first layer "H_m" and total sorption of the multilayers "H_q", in [J/mol]:

$$C = C_0 \times exp\left(\frac{H_l - H_m}{RT}\right) \tag{11}$$

$$K = K_0 \times exp\left(\frac{H_l - H_q}{RT}\right) \tag{12}$$

TABLE 8 GAB variable values

GAB modelization		Sorption				Desorption			
		X_{12}	C	K	RMSE	X_{12}	C	K	RMSE
BEA	TRR	1.470×10^{-04}	$2.00\times10^{+01}$	1.000	1.21×10^{-04}	1.846×10^{-04}	$2.00\times10^{+01}$	0.995	6.15×10^{-05}
	LMA	1.425×10^{-04}	$2.17\times10^{+06}$	1.001	1.14×10^{-04}	1.841×10^{-04}	$3.76\times10^{+06}$	0.995	5.21×10^{-05}
BOR	TRR	1.232×10^{-04}	$2.02\times10^{+00}$	1.002	4.03×10^{-05}	1.902×10^{-04}	9.38×10^{-01}	0.993	3.58×10^{-05}
	LMA	1.155×10^{-04}	$3.03\times10^{+00}$	1.004	1.94×10^{-05}	2.013×10^{-04}	7.75×10^{-01}	0.992	1.16×10^{-05}
BRE	TRR	1.611×10^{-04}	$2.00\times10^{+01}$	0.960	9.68×10^{-05}	1.883×10^{-04}	$2.00\times10^{+01}$	0.950	8.97×10^{-05}
	LMA	1.525×10^{-04}	$4.02\times10^{+06}$	0.963	6.28×10^{-05}	1.836×10^{-04}	$3.58\times10^{+06}$	0.952	5.70×10^{-05}
EUV	TRR	8.322×10^{-05}	$2.00\times10^{+01}$	0.989	7.37×10^{-05}	1.030×10^{-04}	$1.28\times10^{+01}$	0.983	6.98×10^{-05}
	LMA	8.231×10^{-05}	$3.20\times10^{+06}$	0.990	5.56×10^{-05}	1.099×10^{-04}	$2.69\times10^{+06}$	0.979	3.65×10^{-05}
NOG	TRR	1.777×10^{-04}	$2.00\times10^{+01}$	1.007	1.28×10^{-04}	2.920×10^{-04}	$2.00\times10^{+01}$	0.999	1.20×10^{-04}
	LMA	1.774×10^{-04}	$2.25\times10^{+06}$	1.007	3.05×10^{-05}	2.937×10^{-04}	$1.43\times10^{+01}$	0.999	2.96×10^{-05}
NOY	TRR	9.696×10^{-04}	$2.00\times10^{+01}$	0.958	4.70×10^{-04}	1.340×10^{-03}	$2.00\times10^{+01}$	0.934	4.40×10^{-04}
	LMA	9.506×10^{-04}	$5.23\times10^{+06}$	0.959	2.63×10^{-04}	1.303×10^{-03}	$9.17\times10^{+06}$	0.936	2.34×10^{-04}
PAU	TRR	5.826×10^{-05}	$2.00\times10^{+01}$	0.994	4.49×10^{-05}	6.182×10^{-05}	$2.00\times10^{+01}$	0.992	4.21×10^{-05}
	LMA	5.867×10^{-05}	$2.39\times10^{+06}$	0.994	4.03×10^{-05}	6.599×10^{-05}	$2.25\times10^{+06}$	0.990	3.23×10^{-05}
SVF	TRR	1.519×10^{-04}	$1.05\times10^{+01}$	1.011	1.12×10^{-04}	3.292×10^{-04}	9.38×10^{-01}	1.000	8.90×10^{-05}
	LMA	1.586×10^{-04}	$2.10\times10^{+06}$	1.010	1.17×10^{-04}	2.893×10^{-04}	$2.28\times10^{+00}$	1.002	1.22×10^{-04}
SAV	TRR	1.317×10^{-04}	$7.53\times10^{+00}$	1.009	1.43×10^{-04}	2.492×10^{-04}	$5.65\times10^{+00}$	0.999	1.26×10^{-04}
	LMA	1.348×10^{-04}	$2.03\times10^{+06}$	1.009	8.91×10^{-05}	2.266×10^{-04}	$1.66\times10^{+06}$	1.000	4.36×10^{-05}
TER	TRR	1.102×10^{-04}	$1.02\times10^{+01}$	1.004	9.34×10^{-05}	1.540×10^{-04}	$2.00\times10^{+01}$	0.997	8.29×10^{-05}
	LMA	1.045×10^{-04}	$1.71\times10^{+06}$	1.005	1.84×10^{-05}	1.530×10^{-04}	$8.20\times10^{+05}$	0.997	2.03×10^{-05}
TUF	TRR	6.686×10^{-03}	$2.99\times10^{+00}$	0.915	2.74×10^{-04}	1.370×10^{-02}	$1.59\times10^{+00}$	0.824	2.74×10^{-04}
	LMA	6.694×10^{-03}	$2.98\times10^{+00}$	0.915	6.94×10^{-04}	1.376×10^{-02}	$1.59\times10^{+00}$	0.823	6.92×10^{-04}
VPG	TRR	1.047×10^{-03}	$9.52\times10^{+00}$	0.943	5.05×10^{-04}	1.441×10^{-03}	$9.94\times10^{+00}$	0.914	4.36×10^{-04}
	LMA	1.011×10^{-03}	$5.52\times10^{+06}$	0.945	2.37×10^{-04}	1.350×10^{-03}	$2.77\times10^{+06}$	0.920	1.84×10^{-04}

Let us note that the RMSE values are low with good model performance. The modeled curves closely follow the experimental points (**Fig. 7**).

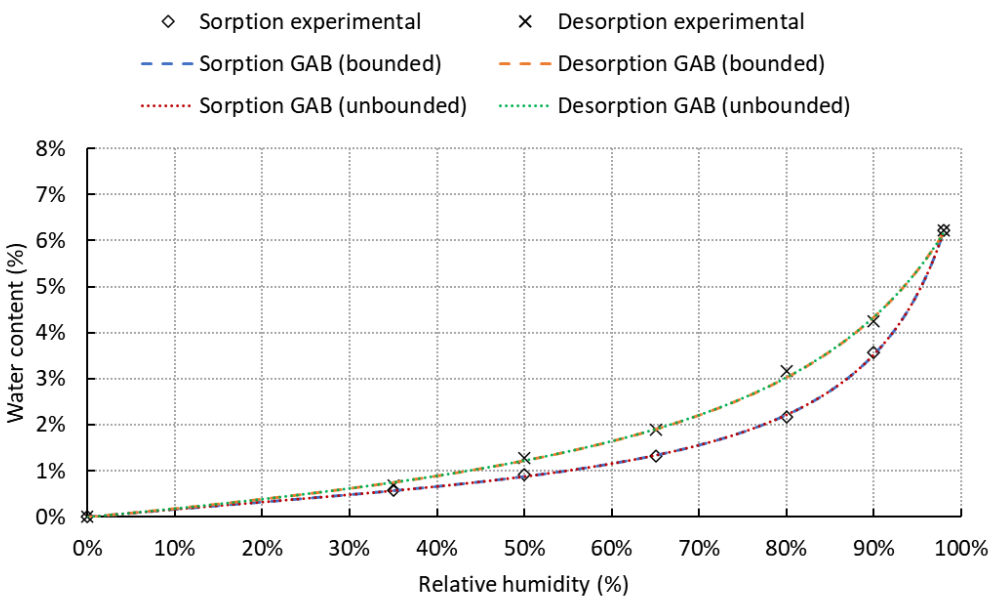

Fig. 7 Example of modeled sorption and desorption curves (TUF stone)

Variable "*K*" varies slightly (0.915 to 1.011) while variable "*C*" sometimes has very high values, according to the LMA algorithm. Variable "X_{12}", which corresponds to water content [kg/kg], is relatively low; its maximum is 0.67% in adsorption and 1.38% in desorption for the TUF stone, which means that the monolayer is being rapidly saturated. The values of these variables are of the same order of magnitude as those in the literature on mineral building materials (Colinart et al. 2017; Poyet and Charles 2009; Issaadi et al. 2015; Poyet 2009).

Hydric transfer coefficients

The determination of water vapor permeability and sorption isotherms entails calculating the water transfer coefficients, which are used in the diffusion equations of vapor or liquid in materials and therefore essential to modeling the coupled heat and moisture transfers. Vapor diffusion is governed by the vapor pressure gradient; it gradually decreases until capillary condensation. At this point, liquid diffusion, mainly governed by the capillary pressure, takes over. Fick's and Darcy's laws explain the phenomena from which the following relationships are derived.

The vapor diffusion coefficient "Dv" [m²/s] is calculated from: the vapor permeability of the material "δ" [kg/(m.s.Pa)], the saturating vapor pressure "$p_{v,sat}$" [Pa], the sorption isotherm tangent "ξ" [kg/kg], and the dry bulk density "ρ_0". This calculation serves to consider water content "w_v", in [kg/m³].

$$Dv(w_v) = \frac{\delta \times p_{v,sat}}{\xi \times \rho_0} \tag{13}$$

The liquid diffusion coefficient "Dl" [m²/s] can be estimated by the following simplified relation (Künzel 1995), where "A" is the water absorption coefficient [kg/(m².s$^{1/2}$)] and "w_f" [kg/m³] the water content at capillary saturation.

$$Dl(w_v) = 3{,}8 \times \left(\frac{A}{w_f}\right)^2 \times 1000^{(w_v - w_f)-1} \tag{14}$$

Total diffusion coefficient "Dw" [m²/s] can be expressed as the sum of vapor and liquid diffusions:

$$Dw = Dv + Dl \tag{15}$$

TABLE 9 provides tabulated values for using these data to model mass, or coupled heat and moisture transfers.

TABLE 9 Tabulated values of the total water diffusion coefficient "Dw" [m²/s].

Stone	25%RH	50%RH	70%RH	80%RH	90%RH	95%RH	@wf
BEA	8.37×10^{-08}	4.63×10^{-08}	2.72×10^{-08}	2.13×10^{-08}	1.83×10^{-08}	1.88×10^{-08}	1.57×10^{-05}
BOR	1.88×10^{-08}	1.19×10^{-08}	5.83×10^{-09}	3.68×10^{-09}	2.43×10^{-09}	2.31×10^{-09}	1.78×10^{-06}
BRE	6.42×10^{-08}	3.48×10^{-08}	1.93×10^{-08}	1.42×10^{-08}	1.11×10^{-08}	1.06×10^{-08}	8.59×10^{-06}
EUV	1.38×10^{-08}	6.38×10^{-09}	3.03×10^{-09}	1.98×10^{-09}	1.36×10^{-09}	1.27×10^{-09}	9.80×10^{-07}
NOG	9.50×10^{-08}	4.44×10^{-08}	1.85×10^{-08}	1.05×10^{-08}	5.85×10^{-09}	5.08×10^{-09}	3.98×10^{-06}
NOY	1.38×10^{-08}	6.86×10^{-09}	3.17×10^{-09}	1.97×10^{-09}	1.25×10^{-09}	1.15×10^{-09}	5.69×10^{-07}
PAU	2.15×10^{-07}	1.01×10^{-07}	4.29×10^{-08}	2.43×10^{-08}	1.30×10^{-08}	1.02×10^{-08}	8.28×10^{-06}
SVF	1.79×10^{-07}	9.87×10^{-08}	5.83×10^{-08}	4.62×10^{-08}	4.04×10^{-08}	4.30×10^{-08}	3.62×10^{-05}
SAV	1.54×10^{-08}	7.26×10^{-09}	3.07×10^{-09}	1.75×10^{-09}	9.89×10^{-10}	8.73×10^{-10}	6.11×10^{-07}
TER	6.95×10^{-08}	3.21×10^{-08}	1.30×10^{-08}	7.01×10^{-09}	3.50×10^{-09}	2.78×10^{-09}	2.14×10^{-06}
TUF	7.76×10^{-09}	7.55×10^{-09}	7.76×10^{-09}	8.65×10^{-09}	1.16×10^{-08}	1.62×10^{-08}	4.61×10^{-06}
VPG	6.67×10^{-09}	3.63×10^{-09}	2.04×10^{-09}	1.55×10^{-09}	1.34×10^{-09}	1.47×10^{-09}	7.08×10^{-07}

Results obtained show comparable patterns for all rocks, which feature a similar behavior (**Fig. 8**). For example, capillary condensation seems to occur past 95% RH for all twelve rocks. Above this relative humidity threshold, liquid diffusion increases rapidly. Keep in mind however that the y-axis scale is logarithmic in **Fig. 8**. The absolute values of the coefficients are not identical; water, in liquid or vapor form, can flow more or less easily through the pore network of limestones.

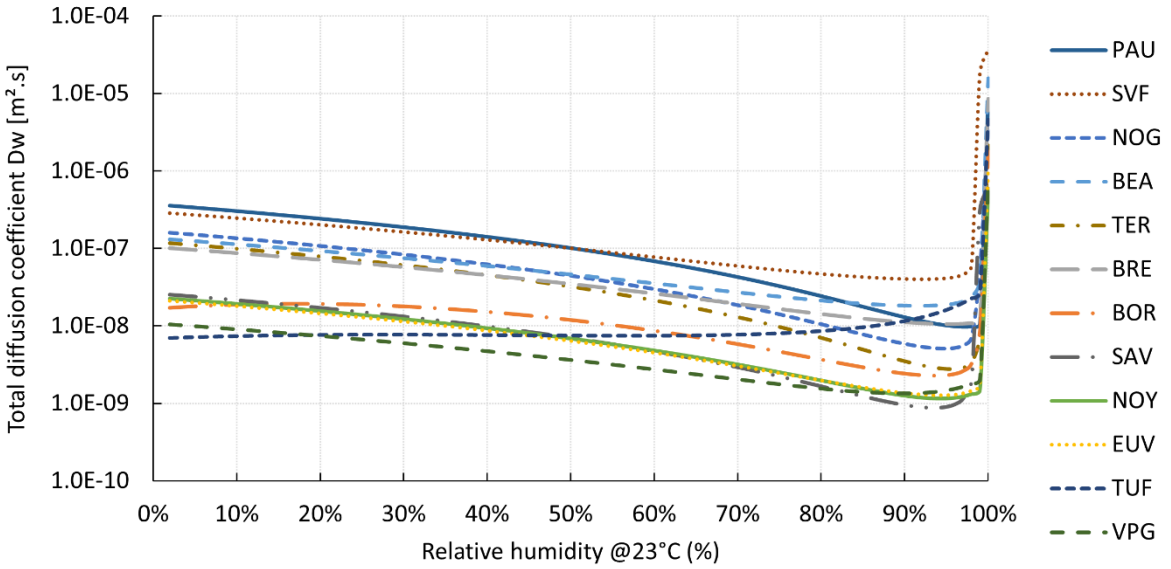

Fig. 8 Total diffusion coefficient

These coefficients depend not only on the water vapor permeability of the materials "δ" [kg/(m.s.Pa)], but also on their water storage capacity "ζ" [kg/kg]. Some stones are rather permeable to water vapor and able to store a large amount of it, e.g. TUF. Such stones are then found with relatively low coefficients. In contrast, the PAU stone has a water vapor permeability slightly lower than the average of the studied stones, yet with a very low water storage capacity. Its mass diffusion coefficients are therefore quite high; however, these coefficients also depend on water content, and stones with a higher maximum water content will be able to diffuse a greater amount of moisture.

THERMAL CHARACTERIZATION

Conductivity and heat capacity

Thermal conductivity has been deduced from the thermal resistance test, as carried out according to EN 12664 (CEN 2001). This test has been adapted to also determine heat capacity. The characterization method protocol calls for imposing a different temperature on the two largest faces of a specimen. We used two thermostatic baths (Huber, Offenburg, Germany) with a range of -20°C to +200°C and accuracy of ±0.1°C connected to two exchange plates. A HP 34401 (Hewlett-Packard, Pao Alto, California) data acquisition system recorded the measurements. We chose a commonly used temperature difference of 10°C between those two faces, and an average temperature of 20°C. This temperature corresponds to the ambient conditions in the laboratory, which contributes to limit the thermal losses through the insulated periphery of the specimen. Factory calibrated heat flux sensors (thermal fluxmeters, Captec, Lille, France) and temperature sensors (T-type thermocouples) were placed between the specimen and the plates. Measurements are recorded simultaneously over a sufficiently long period until reaching steady-state. Thermal resistance "R" [(m².K)/W] can be deduced from the temperature difference "ΔT" [K] and surface heat flux "φ" [W/m²]. Next, thermal conductivity "λ" [W/(m.K)] is deduced from the specimen thickness "e" [m]

$$R = \frac{\Delta T}{\varphi} \tag{16}$$

$$\lambda = \frac{e}{R} \tag{17}$$

Heat capacity is determined by measuring the amount of heat stored by the specimen between two stable thermal states, but at different average temperatures. The amount of heat stored by specimen "Q" [J] can be calculated from the time variation of heat fluxes "ϕ" [W] on both sides of the specimen. Mass heat capacity "c" [J/(kg.K)] is deduced as a function of the temperature difference "ΔT" [K], density "ρ" [kg/m³], surface area "S" [m²] and thickness "e" [m] of the specimen

$$Q = \int_{t_{initial}}^{t_{final}} \Delta\Phi . dt \tag{18}$$

$$c = \frac{Q}{\Delta T . \rho . S . e} \tag{19}$$

Three specimens of the same type of stone were subjected to these two tests. The thermal conductivity and heat capacity of the twelve limestones were determined at two water content levels. To avoid the variation of the water content, the wet test pieces were wrapped in a 15 µm thick layer of vapor-proof polyethylene stretch film. Furthermore, moisture content has been determined before and after the test for both humid and dry stones. The first measurement at 0% water content reveals the stone properties when dry. The second measurement point, close to free water saturation (at atmospheric pressure), indicates the maximum value that characteristics can reach under real use conditions.

For limestones, according to several authors (Çanakci et al. 2007; Wu 2011), the evolution in conductivity and heat capacity versus water content could be expressed by a linear (or quasi-linear) relation. For this reason, only two extreme measurement points were recorded (dry and saturated). The same is true of other materials, for which linear (Asli 2017; Cagnon et al. 2014; Chabriac 2014) or low-growth exponential relationships (Chikhi et al. 2016; Derbal 2014) are expressed. Results are presented in **TABLE 10**.

TABLE 10 Conductivity and heat capacity of limestone

Limestone	w_{dry} [kg/m^3]	λ_{dry} [W/m.K]	λ_{sat} [W/m.K]	w_{sat} [kg/m^3]	c_{dry} [J/kg.K]	c_{sat} [J/kg.K]
BEA	1.00	0.86	1.31	221	738	879
BOR	0.11	1.24	1.40	156	693	946
BRE	0.71	0.86	1.40	200	749	908
EUV	0.35	1.31	1.60	86	704	758
NOG	0.71	0.67	0.99	268	715	1038
NOY	2.15	0.76	1.15	248	720	1035
PAU	0.57	0.95	1.36	207	735	954
SVF	0.92	0.58	1.07	310	740	1180
SAV	0.84	0.94	1.16	103	671	821
TER	0.82	1.02	1.48	204	723	924
TUF	8.10	0.57	1.11	334	743	1387
VPG	3.94	0.78	1.17	203	765	872

The thermal conductivity of dry stone ranged from 0.57 to 1.31 [W/(m.K)], with an average of 0.88±0.12 [W/(m.K)]. The value for water-saturated stones lied between 0.99 and 1.60 [W/(m.K)], with an average of 1.27±0.09 [W/(m.K)]. The thermal mass capacities of dry stones only varied slightly: between 671 and 765 [J/(kg.K)], with an average of 725±13 [J/(kg.K)]. In contrast, when saturated with water, the influence of the heat capacity of water was greater on stones capable of absorbing a large quantity of water.

These values ranged from 758 to 1387 [J/(kg.K)], with an average of 975±88 [J/(kg.K)]; they were of the same order of magnitude as those observed in the literature (Iosif Stylianou et al. 2016; Vigroux 2020; Wu 2011). The values obtained for thermal conductivity were on average 33% lower than those of ISO 10456 (ISO 2007). Some studies made the same observation (Genova et Fatta 2018). In the standard, the heat capacity is set to a constant value of 1000 (J/kg.K), which is 38% higher than the measured values.

Thermal diffusivity and effusivity

The study of unsteady regimes requires knowing the thermal diffusivity "*a*" [m²/s] and effusivity "*b*" [(W.s$^{1/2}$)/(m².K)]; these parameters represent respectively the capacity to transport and store heat. They can be deduced from the previous tests by calculation, thanks to the density, thermal conductivity, and mass heat capacity of the stones.

$$a = \frac{\lambda}{\rho.c} \tag{20}$$

$$b = \sqrt{\lambda.\rho.c} \tag{21}$$

Results are presented in **TABLE 11**. The average thermal diffusivity of dry stone is $6.34\times10^{-7}\pm5.10\times10^{-7}$ [m²/s] and the effusivity is 1094±107 [(W.s$^{1/2}$)/(m².K)]. When saturated with water, these values increase to $6.29\times10^{-7}\pm6.35\times10^{-8}$ [m²/s] and 1600±65 [(W.s$^{1/2}$)/(m².K)].

TABLE 11 Thermal diffusivity and effusivity of limestones

Limestone	a_{dry} [m²/s]	a_{sat} [m²/s]	b_{dry} [(W.s$^{1/2}$)/(m².K)]	b_{sat} [(W.s$^{1/2}$)/(m².K)]
BEA	6.32×10^{-07}	7.11×10^{-07}	1087	1548
BOR	8.05×10^{-07}	6.21×10^{-07}	1383	1776
BRE	5.92×10^{-07}	7.24×10^{-07}	1122	1647
EUV	7.95×10^{-07}	8.62×10^{-07}	1470	1723
NOG	5.46×10^{-07}	4.74×10^{-07}	910	1445
NOY	5.91×10^{-07}	5.42×10^{-07}	992	1556
PAU	6.67×10^{-07}	6.60×10^{-07}	1166	1669
SVF	5.09×10^{-07}	4.85×10^{-07}	810	1533
SAV	7.06×10^{-07}	6.80×10^{-07}	1113	1410
TER	6.83×10^{-07}	7.03×10^{-07}	1240	1766
TUF	5.37×10^{-07}	4.40×10^{-07}	776	1674
VPG	5.44×10^{-07}	6.44×10^{-07}	1055	1458

Water content has a limited influence on thermal diffusivity. The density, heat capacity and thermal conductivity actually increase in sync with the water content. On the contrary, the thermal effusivity of the most porous stones increases significantly when filled with water. Furthermore, thermal diffusivity "*a*" [m²/h] allows estimating the temporal phase shift "*η*" [h] of a wall with thickness "*e*" [m] for a loading lasting a period "*T*" [h]. The phase shift and damping are characteristic phenomena of the thermal inertia of envelopes.

$$\eta = \frac{\sqrt{T}}{2\times\sqrt{\pi}} \times e \times \sqrt{\frac{1}{a}} \tag{22}$$

For example, a wall in massive stone masonry 25 cm thick, the estimated phase shift is 7:15 with a dry limestone representative of the average. By doubling the wall thickness, the time phase shift also doubles. Theoretical results are shown in **TABLE 12** for dry and water-saturated stones. The thickness of massive masonry generally extends from 20 up to 60 cm. The thermal phase shift values here are given for both 25 cm and 50 cm.

TABLE 12 Theoretical thermal phase shift

η(h)	25cm (dry)	50cm (dry)	25cm (sat)	50cm (sat)
BEA	07:14	14:29	06:50	13:40
BOR	06:25	12:50	07:19	14:37
BRE	07:29	14:58	06:46	13:32
EUV	06:28	12:55	06:12	12:24
NOG	07:47	15:35	08:22	16:44
NOY	07:29	14:59	07:49	15:38
PAU	07:03	14:07	07:05	14:11
SVF	08:04	16:08	08:16	16:32
SAV	06:51	13:42	06:59	13:58
TER	06:58	13:56	06:52	13:44
TUF	07:52	15:43	08:41	17:22
VPG	07:49	15:37	07:11	14:22

ESTIMATION OF HYGROTHERMAL PROPERTIES

The wide array of limestone physical properties has advantages as well as disadvantages. Thanks to their varied characteristics and differing aesthetics, natural stones can indeed be used for many applications. Yet this heterogeneity can lead to uncertain product properties. Manufactured materials with reproducible properties do not share this disadvantage. It is important to study hygrothermal couplings and correlations between physical properties in order to estimate the characteristics of natural stones.

Couplings between variables

The geological age of limestones can offer a preliminary indication of density, open porosity and, hence, thermal conductivity (Liu et al. 2011). Older sedimentary rocks are quite often deeper and more compact; their porosities therefore are lower and their densities higher. In our case, the coefficients of determination are low, though this indication does not seem to be very precise (**Fig. 9**). The coefficient of determination measures the quality of the regression. In our case, considering the measurement uncertainties, we can consider that above 0.80 the model may be used to properly predict values of the rock properties. Below this value, it is necessary to take more precautions. These regressions highlight the complexity of the phenomena with water and the influence of the pore network. Some parameters cannot be predicted with a single variable.

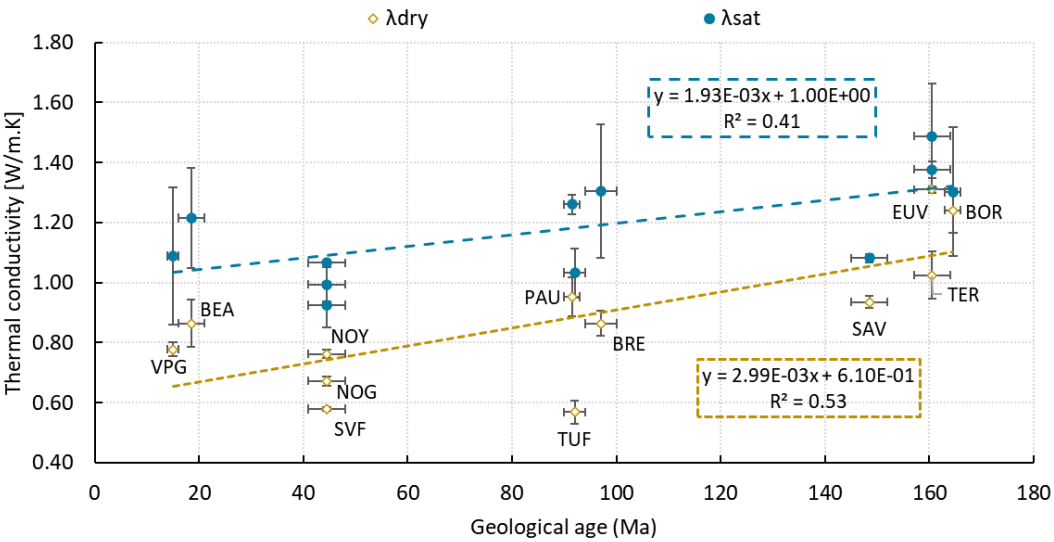

Fig. 9 Thermal conductivity as a function of geological age

Density and open porosity are relatively simple properties to obtain, while still providing a fairly accurate idea of the limestone characteristics, particularly thermal conductivity (**Fig. 10**). Porosity is inversely proportional to density for the studied limestones (**Fig. 2**). However, thermal conductivity is directly dependent on not only the quantity of air trapped by the pore network but also the thermal conductivity of the solid matrix. The latter varies little for the same geological type of rock. The best results are obtained between the thermal conductivity of dry limestone and open porosity, although density is also quite representative.

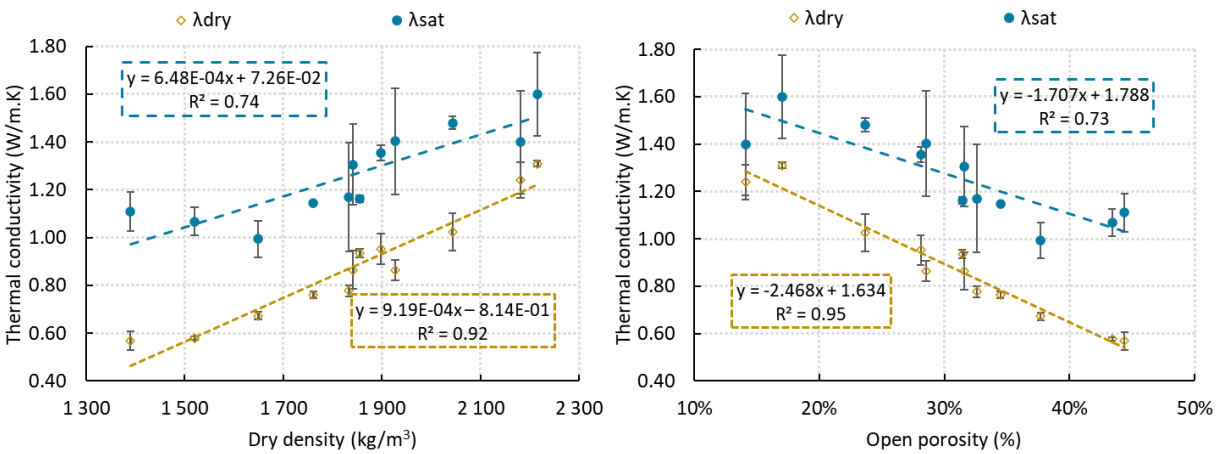

Fig. 10 Thermal conductivity as a function of density and porosity

Thermal diffusivity and effusivity are properties dependent on both conductivity and heat capacity, as well as on density. The relationship between open porosity and density gives good results, especially for dry stones. However, the regression coefficient is lower for water-saturated stones (**Fig. 11**). The pore network differs from stone to stone, as the saturation water content, making linear estimation of thermal properties difficult.

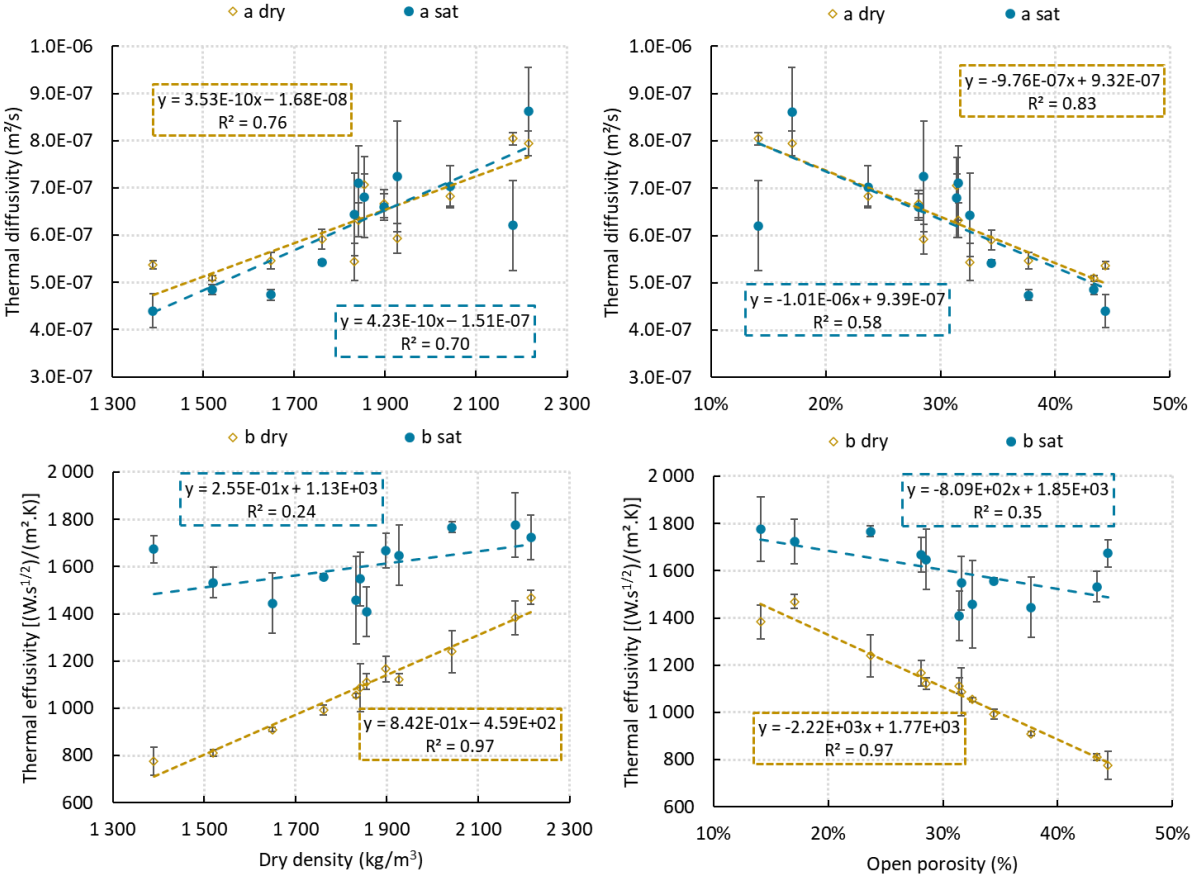

Fig. 11 Thermal diffusivity and effusivity as a function of density and porosity

The same is true for the couple "*ρ.c*", or volumetric heat capacity [J/(m^3.K)]. The coefficients of determination are interesting for dry stones, whether with density or porosity (**Fig. 12**). Conversely, dispersion is much greater for water saturated stones and the R² is lower.

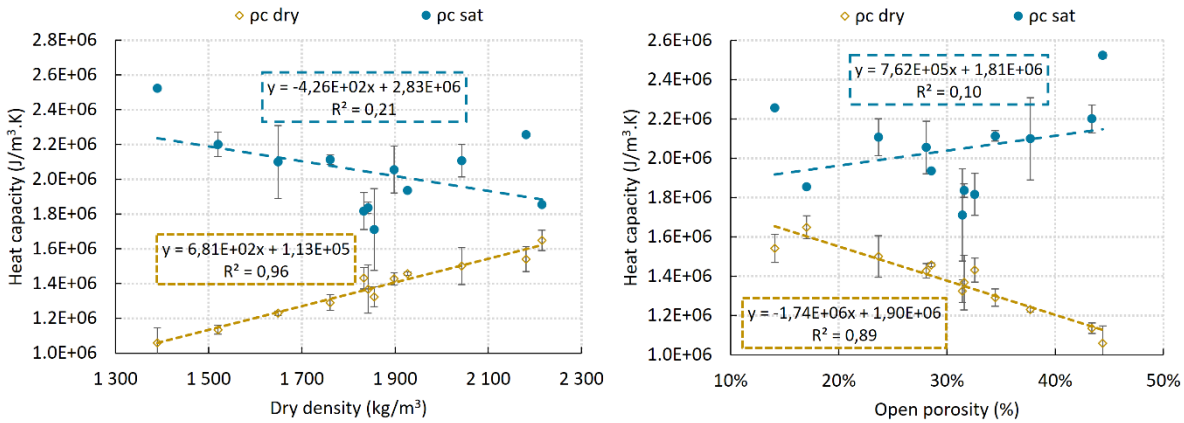

Fig. 12 Heat capacity as a function of density and porosity

Density and open porosity can also provide some information about hydric properties, such as water vapor permeability (Fig. 13).

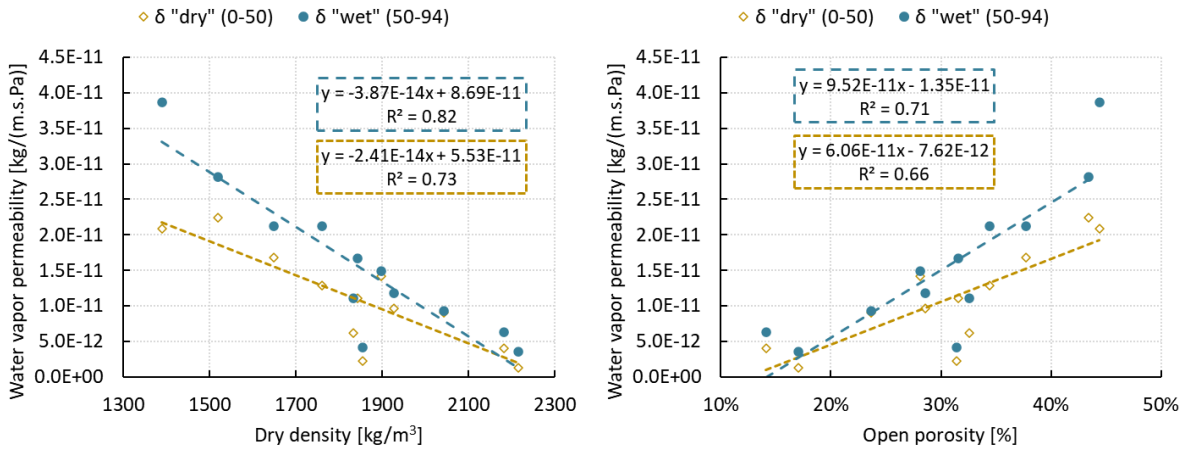

Fig. 13 Water vapor permeability as a function of density, and open porosity

However, these two properties are still not sufficient to estimate characteristics precisely. Water vapor permeability does depend on open porosity, but also on the type of pore network. According to (Vigroux 2020), some parameters such as mercury porosimetry or porosity at 48 h could yield better results. This hypothesis has been verified by observing the exponential relationship between "wet cup" permeability and accessible porosity, whose coefficients of determination are particularly high. (Fig. 14).

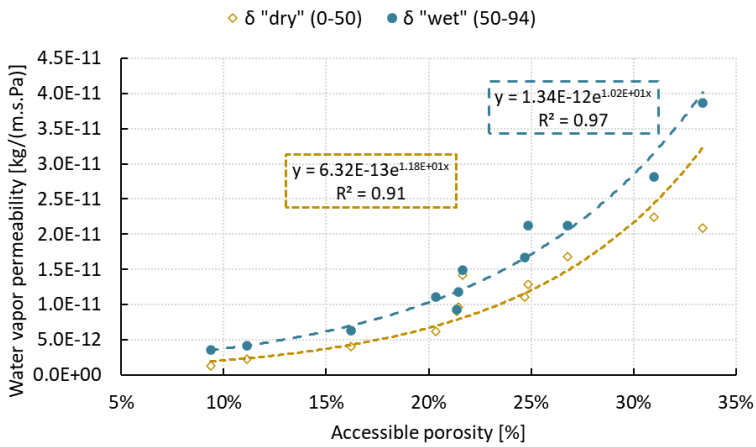

Fig. 14 Water vapor permeability as a function of accessible porosity

Estimation of the properties by classes

The statistical classes previously determined (**TABLE 2**) can now be used to estimate the multi-physical characteristics of limestone. As a reminder, out sampling has included stones of the last three classes, which are representative of rocks used for constructing building walls. The 95% confidence interval (or 90% for water vapor permeability and MBV) is calculated according to the Student's law and number of samples. With some 50 pairs, the database is larger for mechanical properties than for hygrothermal properties. Consequently, representativeness increases with a lower confidence interval. Classes 3 and 5 have only three limestones with known hygrothermal properties. Some characteristics vary significantly within the same class; for example, the MBV of class 5 limestones ranges from 0.56 to 2.66 [g/(m².$\%_{RH}$)] and the water vapor permeability from 2.28×10^{-12} to 2.09×10^{-11} [kg/(m.s.Pa)].

TABLE 13 Properties of limestones by statistical classes

Statistical class	3	4	5
ρ [kg/m^3]	2148 ±12	1836 ±16	1528 ±34
n [%]	20 ±1	32 ±1	44 ±1
Rf [MPa]	6.7 ±0.4	3.5 ±0.2	1.9 ±0.2
Rc [MPa]	37.6 ±4.3	16.1 ±1.7	7.9 ±2.0
λ_{dry} [W/(m.K)]	1.19 ±0.20	0.86 ±0.06	0.61 ±0.08
λ_{sat} [W/(m.K)]	1.49 ±0.14	1.26 ±0.09	1.06 ±0.08
c_{dry} [J/(kg.K)]	707 ±21	730 ±26	733 ±21
c_{sat} [J/(kg.K)]	876 ±139	911 ±59	1202 ±238
δ_{dry} [kg/(m.s.Pa)]	4.82×10^{-12} ±3.70×10^{-12}	1.28×10^{-11} ±3.25×10^{-12}	1.33×10^{-11} ±9.24×10^{-12}
δ_{wet} [kg/(m.s.Pa)]	6.38×10^{-12} ±2.74×10^{-12}	1.73×10^{-11} ±3.81×10^{-12}	2.14×10^{-11} ±1.63×10^{-11}
MBV [g/(m².$\%_{RH}$)]	0.27 ±0.07	0.53 ±0.19	1.29 ±1.12

TABLE 13 lists the global estimations of multi-physical properties of the main limestones used in construction. These data can be applied upstream of construction, as preliminary inputs. Greater precision will be necessary to design the building's structural features or conduct other regulatory technical studies. They should allow simulating heat and moisture transfers in limestone building components more accurately than by using ISO 10456 values (ISO 2007). Indeed, some differences were noticed with this standard, which, by interpolation, gave the following values: Class 3 μ=161 [-] and λ=1.63 [W/m.K] ; Class 4 μ=42 and λ=1.17 ; Class 5 μ=26 and λ=0.72. Heat capacity is set at 1000 [J/kg.K] for many materials, including limestones. Similarly, the water vapor resistance factor "μ" of plaster and coatings is constant, whatever the density. However, several bibliographic references seem to confirm our results (Vigroux 2020; De Kock et al. 2017; Iosif Stylianou et al. 2016; Wu 2011).

CONCLUSION

The main physical and hygrothermal properties of a representative sample of components used in limestone building envelopes have been determined and analyzed. A statistical study based on the physical-mechanical properties of limestones has served to estimate some of their characteristics and group the nearby stones into different categories. This research has provided useful data for the simulation of coupled heat and humidity transfers in walls incorporating natural stone. Such a complete data set is particularly hard to find in the literature. This type of material, which is both local and natural, requires little transformation and is capable of being reused or recycled; it will likely become increasingly widespread. Although difficult to obtain, reliable data are necessary to achieve specific developments in building regulations. The same is true for more specialized technical studies, notably those related to historical buildings. It has been demonstrated that hydric and thermal properties are strongly influenced by both temperature and water content. Note the importance of taking these couplings into account in order to improve the reliability of energy simulations for buildings, but also to preserve structural durability and ensure the comfort and good health of occupants. The limestones studied possess qualities that need to be optimized. Some stones have significant hydric buffering capacities and ideally should be left exposed within the occupied environment to regulate humidity. The thermal properties of limestone demonstrate its ability to store and destock large quantities of heat, and therefore reduce and shift the phase of the thermal stresses imposed on buildings. This multifaceted potential impacts the energy consumption of the dwelling and improves occupants' comfort. Future prospects of this research will focus on the couplings between structural materials and bio-based insulation, by means of a numerical approach, to offer energy-efficient walls with a low environmental impact while respecting the health of occupants.

DATA AVAILABILITY STATEMENT

Data, models, or codes that support the results of this study are available from the corresponding author upon reasonable request.

ACKNOWLEDGEMENTS

This research work was carried out as part of a thesis co-funded by the CTMNC (Technical Center for Natural Construction Materials) and the ANRT (National Association for Research and Technology) in partnership with the LGCgE (laboratory of civil engineering and geo-environment).

REFERENCES

Abadie, M., P. Blondeau, et J. Nicolle. 2013. « Mémento Santé Bâtiment - Qualité de l'air intérieur ». hal-01009964. LaSIE - Université de la Rochelle. Caisse des dépôts.

Abelé, C., B. Abraham, J-L. Salagnac, J. Fontan, D. Quenard, S. Gilliot, et C. Pompéo. 2009. *Transferts d'humidité à travers les parois évaluer les risques de condensation*. Guide Technique G06-02. France: CSTB.

Abhilash, H.N., F. McGregor, Y. Millogo, A. Fabbri, A.D. Séré, J.E. Aubert, et J.C. Morel. 2016. « Physical, Mechanical and Hygrothermal Properties of Lateritic Building Stones (LBS) from Burkina Faso ». *Construction and Building Materials* 125 (octobre): 731-41. https://doi.org/10.1016/j.conbuildmat.2016.08.082.

Akil, Mostafa, Pierre Tittelein, Didier Defer, et Frédéric Suard. 2019. « Statistical Indicator for the Detection of Anomalies in Gas, Electricity and Water Consumption: Application of Smart Monitoring for Educational Buildings ». *Energy and Buildings* 199 (septembre): 512-22. https://doi.org/10.1016/j.enbuild.2019.07.025.

Asli, M. 2017. « Etude des transferts couplés de chaleur et de masse dans les matériaux bio-sourcés : Approches numérique et expérimentale ». Ph.D. thesis, Université d'Artois.

Beck, K. 2006. « Étude des propriétés hydriques et des mécanismes d'altération de pierres calcaires à forte porosité. » Ph.D. thesis, Université d'Orléans.

Blahovec, J., et S. Yanniotis. 2010. « "GAB" Generalised Equation as a Basis for Sorption Spectral Analysis ». *Czech Journal of Food Sciences* 28 (No. 5): 345-54. https://doi.org/10.17221/146/2009-CJFS.

Cagnon, H., J.E. Aubert, M. Coutand, et C. Magniont. 2014. « Hygrothermal Properties of Earth Bricks ». *Energy and Buildings* 80 (septembre): 208-17. https://doi.org/10.1016/j.enbuild.2014.05.024.

Çanakci, H., R. Demirboğa, M. Burhan Karakoç, et O. Şirin. 2007. « Thermal Conductivity of Limestone from Gaziantep (Turkey) ». *Building and Environment* 42 (4): 1777-82. https://doi.org/10.1016/j.buildenv.2006.01.011.

CEN. 2001. « EN 12664:2001 - Thermal performance of building materials and products - Determination of thermal resistance by means of guarded hot plate and heat flow meter methods - Dry and moist products of medium and low thermal resistance. »

———. 2006. « EN 1936:2006 - Natural stone test methods - Determination of real density and apparent density, and of total and open porosity. »

———. 2008. « EN 13755:2008 - Natural stone test methods - Determination of water absorption at atmospheric pressure. »

———. 2011. « EN 772-11:2011 - Methods of test for masonry units - Part 11: Determination of water absorption of aggregate concrete, autoclaved aerated concrete, manufactured stone and natural stone masonry units due to capillary action and the initial rate of water absorption of clay masonry units. »

———. 2015. « EN 771-6:2011+A1:2015 - Specification for masonry units - Part 6: Natural stone masonry units. »

Chabriac, P-A. 2014. « Mesure du comportement hygrothermique du pisé ». Ph.D. thesis, ENTPE - CNRS - LTDS (UMR 5513). HAL Id: tel-01413611.

Chikhi, A. 2016. « Etude du Comportement Thermo-Hydrique des Parois des Bâtiments. Influence des Effets de l'Etat Hygrothermique et des Propriétés Thermo-Physiques ». Ph.D. thesis, Université de Constantine - Université de Bretagne Sud.

Colinart, T., P. Glouannec, M. Bendouma, et P. Chauvelon. 2017. « Temperature Dependence of Sorption Isotherm of Hygroscopic Building Materials. Part 2: Influence on Hygrothermal Behavior of Hemp Concrete ». *Energy and Buildings* 152 (octobre): 42-51. https://doi.org/10.1016/j.enbuild.2017.07.016.

CTMNC. 2021. « Lithoscope, la lithothèque du CTMNC. » Lithoscope la base de données des pierres naturelles françaises du CTMNC. 2021. https://lithoscopectmnc.com/.

De Kock, Tim, Aurélie Turmel, Gilles Fronteau, et Veerle Cnudde. 2017. « Rock Fabric Heterogeneity and Its Influence on the Petrophysical Properties of a Building Limestone: Lede Stone (Belgium) as an Example ». *Engineering Geology* 216 (janvier): 31-41. https://doi.org/10.1016/j.enggeo.2016.11.007.

Derbal, R. 2014. « Développement d'une méthode inverse de caractérisation thermique. Application à l'estimation des propriétés thermophysiques et hydriques des matériaux de construction. » Ph.D. thesis, Université d'Artois.

Dessandier, D., J. Benharrous, F. Michel, et D. Pallix. 2014. « Mémento sur l'industrie française des roches ornementales et de construction ». Rapport final BRGM/RP-62417-FR. BRGM-SNROC-CTMNC.

Dunham, R. J. 1962 « Classification of carbonate rocks according to depositional texture. » In Proc., Classification of Carbonate Rocks - A Symp. Tulsa, OK: American Association of Petroleum Geologists. https://doi.org/10.1306/M1357.

Folk, R. L. 1959. « Practical petrographic classification of limestones. » AAPG Bull. 43 (1) : 1-38. https://doi.org/10.1306/0BDA5C36-16BD-11D7-8645000102C1865D.

French Republic. 2018. LOI n°2018-1021 du 23 novembre 2018 portant évolution du logement, de *l'aménagement et du numérique (1)*. Vol. NOR : TERL1805474L.

———. 2021. *Projets de décret et arrêtés relatifs aux exigences de performance énergétique et environnementale, et à la méthode de calcul associée, pour la réglementation environnementale 2020 (RE2020)*. http://www.consultations-publiques.developpement-durable.gouv.fr/projets-de-decret-et-arretes-relatifs-aux-a2330.html.

Genova, Enrico, et Giovanni Fatta. 2018. « The Thermal Performances of Historic Masonry: In-Situ Measurements of Thermal Conductance on Calcarenite Stone Walls in Palermo ». *Energy and Buildings* 168 (juin): 363-73. https://doi.org/10.1016/j.enbuild.2018.03.009.

Iosif Stylianou, I., S. Tassou, P. Christodoulides, I. Panayides, et G. Florides. 2016. « Measurement and Analysis of Thermal Properties of Rocks for the Compilation of Geothermal Maps of Cyprus ». *Renewable Energy* 88 (avril): 418-29. https://doi.org/10.1016/j.renene.2015.10.058.

ISO. 2007. « ISO 10456:2007 - Building materials and products - Hygrothermal properties - Tabulated design values and procedures for determining declared and design thermal values ».

———. 2013. « ISO 12571:2013 : Hygrothermal performance of building materials and products - Determination of hygroscopic sorption properties. »

———. 2016. « ISO 12572:2016 - Hygrothermal performance of building materials and products - Determination of water vapour transmission properties - Cup method. »

Issaadi, N., A. Nouviaire, R. Belarbi, et A. Aït-Mokhtar. 2015. « Moisture Characterization of Cementitious Material Properties: Assessment of Water Vapor Sorption Isotherm and Permeability Variation with Ages ». *Construction and Building Materials* 83 (mai): 237-47. https://doi.org/10.1016/j.conbuildmat.2015.03.030.

Jannot, Y., A. Kanmogne, A. Talla, et L. Monkam. 2006. « Experimental Determination and Modelling of Water Desorption Isotherms of Tropical Woods: Afzelia, Ebony, Iroko, Moabi and Obeche ». *Holz Als Roh- Und Werkstoff* 64 (2): 121-24. https://doi.org/10.1007/s00107-005-0051-2.

Kourkoulis, S. K., éd. 2006. *Fracture and Failure of Natural Building Stones: Applications in the Restoration of Ancient Monuments ; [Symposium Was Organized in the Frame of the « 16th European Conference on Fracture » , Took Place in Alexandroupolis, Hellas on July 3-7, 2006 in Democritus University of Thrace]*. Greece: Springer.

Künzel, H. M. 1995. *Simultaneous Heat and Moisture Transport in Building Components: One- and Two-Dimensional Calculation Using Simple Parameters*. Fraunhofer Institute of building physics. Germany. http://publica.fraunhofer.de/eprints/urn_nbn_de_0011-px-566563.pdf.

Litti, Giovanni, Somayeh Khoshdel, Amaryllis Audenaert, et Johan Braet. 2015. « Hygrothermal Performance Evaluation of Traditional Brick Masonry in Historic Buildings ». *Energy and Buildings* 105 (octobre): 393-411. https://doi.org/10.1016/j.enbuild.2015.07.049.

Liu, S., C. Feng, L. Wang, et C. Li. 2011. « Measurement and Analysis of Thermal Conductivity of Rocks in the Tarim Basin, Northwest China ». *Acta Geologica Sinica - English Edition* 85 (3): 598-609. https://doi.org/10.1111/j.1755-6724.2011.00454.x.

Lucchi, Elena. 2017. « Thermal Transmittance of Historical Stone Masonries: A Comparison among Standard, Calculated and Measured Data ». *Energy and Buildings* 151 (septembre): 393-405. https://doi.org/10.1016/j.enbuild.2017.07.002.

Martinet, G., et B. Quénée. 2008. « Pierres de construction - Utilisation, études et diagnostics ». COR404 V1. Techniques de l'ingénieur.

Mendell, M. J., J. M. Macher, et K. Kumagai. 2018. « Measured Moisture in Buildings and Adverse Health Effects: A Review ». *Indoor Air* 28 (4): 488-99. https://doi.org/10.1111/ina.12464.

Ortiz, M., L. Itard, et P. M. Bluyssen. 2020. « Indoor Environmental Quality Related Risk Factors with Energy-Efficient Retrofitting of Housing: A Literature Review ». *Energy and Buildings* 221 (août): 110102. https://doi.org/10.1016/j.enbuild.2020.110102.

Pascucci, M., and E. Lucchi. 2016. « 2D-Hygrothermal Simulation of Historical Solid Walls. » In Proc., Int. Conf. on Computer Aided Architectural Design - CAADence in architecture. Bolzano, Italy: Institute for Renewable Energy. https://doi.org/10.3311/CAADence.1640.

Popielski, A. C., Z. Heidari, et C. Torres-Verdín. 2012. « Rock Classification from Conventional Well Logs in Hydrocarbon-Bearing Shale ». In *All Days*, SPE-159255-MS. San Antonio, Texas, USA: SPE. https://doi.org/10.2118/159255-MS.

Poyet, S., et S. Charles. 2009. « Temperature Dependence of the Sorption Isotherms of Cement-Based Materials: Heat of Sorption and Clausius–Clapeyron Formula ». *Cement and Concrete Research* 39 (11): 1060-67. https://doi.org/10.1016/j.cemconres.2009.07.018.

Poyet, Stéphane. 2009. « Experimental Investigation of the Effect of Temperature on the First Desorption Isotherm of Concrete ». *Cement and Concrete Research* 39 (11): 1052-59. https://doi.org/10.1016/j.cemconres.2009.06.019.

Rode, C, R.H. Peuhkuri, L.H. Mortensen, K.K. Hansen, B. Time, A. Gustavsen, T. Ojanen, et al. 2005. *Moisture Buffering of Building Materials*. Technical University of Danmark, Department of Civil Engineering. BYG Report, No. R-126. Danmark. https://backend.orbit.dtu.dk/ws/portalfiles/portal/2415500/byg-r126.pdf.

Rousset Tournier, B., Y. Geraud, et D. Jeannette. 2001. « Transferts par capillarité et évaporation dans des roches - rôle des structures de porosité ». Ph.D. thesis, Université Louis Pasteur.

Sing. K. S. W. 1985. « Reporting physisorption data for gas/solid systems with special reference to the determination of surface area and porosity. » Int. Union Pure Appl. Chem. 57 (4): 603-619. https://doi.org/10.1351/pac198557040603.

UNFCCC. 2021. « Nationally Determined Contributions under the Paris Agreement. Synthesis Report by the Secretariat ». In *CMA 3*, FCCC/PA/CMA/2021/2:32.

Vigroux, M. 2020. « Influence de la microstructure et de la minéralogie sur l'endommagement mécanique des pierres de construction utilisées dans le patrimoine bâti sous l'effet de conditions environnementales sévères ». Ph.D. thesis, Université de Cergy-Pontoise.

Wu, T. 2011. « Formalisme des impédances thermiques généralisées. Application à la caractérisation thermique de parois de bâtiments ». Ph.D. thesis, Université d'Artois.

Zhao, J., et R. Plagge. 2015. « Characterization of Hygrothermal Properties of Sandstones—Impact of Anisotropy on Their Thermal and Moisture Behaviors ». *Energy and Buildings* 107 (novembre): 479-94. https://doi.org/10.1016/j.enbuild.2015.08.033.